

A New Heterometallic 3d-3d Transition Metal Oxo-cluster {Cu^{II}₆Mn^{III}}: Synthesis, Crystal Structure and Magnetic Property^①

WANG Yi-Man PENG Zhi-Wei LIAO Jia-Min LI Ao

LIU Yuan-Yan ZHANG Jing-Jing ZHOU Nian

LI Xu-Dong LI Shu MENG Wei^②

(Department of Materials & Chemistry Engineering, Hunan City University, Yiyang 413000, China)

ABSTRACT A new transition metal-antimony oxo-cluster based compound has been synthesized in water under room temperature. Its formula is Na₆[Cu₆MnSb₆(μ₃-OH)₂(OH)(μ₄-O)₆(tartrate)₆] · 20H₂O (**1**), where tartrate represents *rac*-tartaric acid. It was characterized by elemental analysis, infrared spectrum and X-ray single-crystal diffraction. The compound crystallizes in the monoclinic system, space group *P*2₁/*n*. Structural analyses revealed that two Sb₃(μ₃-O)(tartrate)₃ scaffolds sandwich a Cu^{II}₆Mn^{III} middle layer to form the cluster. In the middle layer, all the seven metal ions lie in an almost regular hexagon, with Mn^{III} ion in the center and six Cu^{II} ions along the edges of the hexagon. As a 4-connected node, each cluster is interlinked to its nearest four {Cu₆Mn} neighbors through Na⁺, generating a 3D supramolecular framework. The temperature-dependent magnetic susceptibilities indicated dominating antiferromagnetic interactions in **1** with *J*_{Cu–Cu} = 176.34 and *J*_{Cu–Mn} = –14.44 cm^{–1}.

Keywords: dipotassium bis(μ-tartrato)-diantimony(III) ligand, heterometallic transition metal oxo-cluster, crystal structure, magnetic study; DOI: 10.14102/j.cnki.0254-5861.2011-3229

1 INTRODUCTION

Heterometallic transition metal oxo-clusters have recently attracted great attention due to their intriguing geometrical characteristics and fascinating physical properties^[1–7]. One of the driving forces for this is to explore the exchange interactions among multiple non-equivalent spin carrying centers in a single molecule^[8–10]. Between the nearest nonequivalent neighboring spin carriers, the magnetic interactions may be ferromagnetic or antiferromagnetic^[11, 12]. Especially when the metal ions are strongly anisotropic, the combination with various hetero-spin carriers can lead to a new generation of molecule-based magnetic materials^[13, 14]. In addition, different metal ions to assemble these clusters can induce different functionality, such as the combination of magnetic, optical, chiral and biological activities with catalytic properties^[15–18].

Previously, we have been interested in using the inorganic ligand pool, K₂Sb₂L₂ (H₄L = tartaric acid), namely

dipotassium bis(μ-tartrato)-diantimony(III), as a starting material for the synthesis of pure divalent late transition metal-oxo clusters^[18, 19]. The K₂Sb₂L₂ ligand was selected to construct high nuclearity oxo-clusters because of two reasons. On one hand, it can undergo decomposition and recombination to form two types of scaffolds in an aqueous medium. On the other hand, tartaric acid contains both alkoxide and carboxylate groups. In this research field, Jacobson and co-workers discovered a series of sandwich-type clusters by using the enantiopure forms of K₂Sb₂L₂^[20–22]. Meanwhile, Huang et al. also reported several transition metal-antimony oxo-cluster^[2]. However, Cu(II)/Mn(III) ions sandwiched by {Sb₃(μ₃-O)} have not yet been reported. In this work, we present the synthesis, characterization and magnetism of an anionic cluster, Na₆[Cu₆MnSb₆(μ₃-OH)₂(OH)(μ₄-O)₆(tartrate)₆] · 20H₂O (**1**).

2 EXPERIMENTAL

Received 21 April 2021; accepted 28 May 2021 (CCDC 2077972)

① Supported by the National Natural Science Foundation of China (No. 22001064), the Natural Science Foundation of Hunan Province (No. 2020JJ4155), the Hunan Province College Students' Innovation Entrepreneurship Training Program (2020 No. 3373, 2021 No. 3340), and the Scientific Research Project of Hunan Province Department of Education (No. 20B105)

② Corresponding author. E-mail: mengw198503@163.com

2.1 General materials and methods

All reagents and solvents were of AR grade and used without further purification. Infrared spectrum test was measured on a WQF-410 FTIR spectrometer with wave number of 500~4000 cm⁻¹. Thermogravimetric analysis (TGA) measurements were carried out using a DSC/TG pan A1203 system in N₂ flow at a heating rate of 10 °C/min. Elemental analyses were performed (C, H) by Thermo Scientific FLASH 2000 elemental analyzer; Mn, Cu and Na were analyzed on a Varian (720) ICP atomic emission spectrometer. Single-crystal X-ray analyses were carried out at room temperature on a Siemens SMART platform diffractometer outfitted with an Apex II area detector and monochromatized Mo-K α radiation ($\lambda = 0.71073$ Å). Powder X-ray diffraction patterns were gathered in the 2θ range of 5~80 ° at room temperature on a Rigaku D/Max 2500 diffractometer. Magnetic susceptibility was measured on a MPMS RSO Instrument.

2.2 Synthesis of Na₆[Cu₆MnSb₆(μ_3 -OH)₂(OH)(μ_4 -O)₆(tartrate)₆] 20H₂O (1)

A mixture of Cu(OAc)₂ (0.62 mmol), Mn(OAc)₂ (0.31 mmol) and *rac*-K₂Sb₂(tartrate)₂ (0.62 mmol) was added to a sodium acetate/acetic acid buffer solution (pH 5.5, 0.5 M NaOAc/HOAc, 10 mL). The solution was stirred for 8 h and filtered, and the gray-green filtrate was left undisturbed to concentrate slowly by evaporation. Green crystals of **1** were obtained with the yield of 46% (based on Cu) after three

weeks. Anal. Calcd. for C₂₄H₅₅Cu₆MnNa₆O₆₅Sb₆: C, 10.71; H, 2.05; Cu, 14.18; Mn, 2.04; Na, 5.13; Sb, 27.16. Found: C, 10.63; H, 2.01; Cu, 14.25; Mn, 2.11; Na, 5.05; Sb, 27.22. IR (KBr pellet, cm⁻¹): 1613 (s), 1418 (s), 1366 (s), 1110 (s), 1069 (m), 925 (w), 905 (w), 854 (m), 751 (w), 648 (s), 545 (w), 515 (w).

2.3 Crystal structure determination

A green needle single crystal of **1** with dimensions of 0.43mm × 0.40mm × 0.38mm was selected and mounted on a glass fiber. Data collection was performed at 294 K on a Smart Apex II CCD with graphite-monochromated MoK α radiation ($\lambda = 0.71073$ Å). The structure of **1** was solved by direct methods and refined by full-matrix least-squares method on F^2 using the SHELXTL-97 crystallographic software package^[23]. More details on the crystallographic studies as well as atomic displacement parameters are given in the CIF files. All carbon-bonded hydrogen atoms were placed in geometrically calculated positions; hydrogen atoms in water molecules were not assigned or directly included in the molecular formula. Compound **1** crystallizes out in monoclinic, space group $P2_1/n$ with $a = 16.8688(10)$, $b = 9.4734(5)$, $c = 22.5825(14)$ Å, $V = 3599.8(3)$ Å³, $Z = 2$, C₂₄H₅₅Cu₆MnNa₆O₆₅Sb₆, $M_r = 2688.30$, $D_c = 2.480$ g/cm³, $F(000) = 2580$, $\mu(\text{MoK}\alpha) = 4.275$ mm⁻¹, the final $R = 0.0317$ and $wR = 0.0827$ ($w = 1/[\sigma^2(F_o^2) + (0.0312P)^2 + 21.8403P]$, where $P = (F_o^2 + 2F_c^2)/3$), $S = 1.062$. The selected bond lengths and bond angles are reported in Table 1.

Table 1. Selected Bond Lengths (Å) and Bond Angles (°)

Bond	Dist.	Bond	Dist.	Bond	Dist.
Mn(1)–O(19)	1.950(2)	Mn(1)–O(20)	2.002(4)	Mn(1)–O(21)	2.128(1)
Cu(1)–O(15)	1.943(7)	Cu(1)–O(15)	1.961(6)	Cu(1)–O(20)	1.976(3)
Cu(1)–O(7)	2.585(6)	Cu(1)–O(12)	2.005(6)	Cu(1)–O(19)	2.364(4)
Cu(2)–O(3)	1.948(0)	Cu(2)–O(6)	1.948(2)	Cu(2)–O(13)	2.687(0)
Cu(2)–O(18)	2.016(7)	Cu(2)–O(20)	2.408(1)	Cu(2)–O(21)	1.968(9)
Cu(3)–O(1)	2.542(0)	Cu(3)–O(6)	2.041(0)	Cu(3)–O(9)	1.978(1)
Cu(3)–O(12)	1.990(9)	Cu(3)–O(21)	2.278(0)	Cu(3)–O(19)	2.021(0)
Angle	(°)	Angle	(°)	Angle	(°)
O(12)–Cu(1)–O(15)	89.329(1)	O(3)–Cu(2)–O(4)	142.76(7)	O(9)–Cu(3)–O(10)	143.25(6)
O(15)–Cu(1)–O(16)	142.72(1)	O(6)–Cu(2)–O(21)	85.669(1)	O(1)–Cu(3)–O(9)	116.387(1)
O(19)–Mn(1)–O(21)	85.749(1)	O(20)–Mn(1)–O(21)	86.239(1)	O(19)a–Mn(1)–O(20)	86.288(1)

3 RESULTS AND DISCUSSION

3.1 Structure description for Na₆[Cu₆MnSb₆(μ_3 -OH)₂(OH)(μ_4 -O)₆(tartrate)₆] 20H₂O (1)

Compound **1** contains the [Cu₆MnSb₆(μ_3 -OH)₂(OH)(μ_4 -O)₆(tartrate)₆]⁶⁻ cluster ion. In this cluster ion, two

Sb₃(μ_3 -O)(tartrate)₃ scaffolds (Fig. 1a) sandwich a Cu^{II}₆Mn^{III} middle layer to form the cluster ion, a similar arrangement to what was found in the previously reported Cu^{II}₇ cluster^[19, 24]. In the middle layer, all the seven metal ions lie in an almost regular hexagon (Fig. 1b), with Mn^{III} ion in the center and six Cu^{II} ions along the edges of the hexagon. The central

Mn^{III} ion is hexacoordinated in a regular octahedral fashion with the Mn–O bond lengths ranging from 1.950 to 2.128 Å. This unique Mn^{III} ion is bridged to the six surrounding Cu^{II} ions by six μ_4 -O atoms, similar to the arrangement of metal ions in an Anderson cluster^[25]. The oxidation state of the Mn and Cu ions was determined by bond-valence sum (BVS)

calculation (Table 2). Compared with the previously reported Cu^{II}₇ clusters^[18], all of the Cu^{II} ions are six-coordinated, each with five “normal” Cu–O bonds (ca. 1.94~2.40 Å) and one long Cu–O bond (ca. 2.54~2.68 Å). The coordination sphere of six Cu^{II} ions is completed by two μ_4 -O and four other oxygen atoms from two tartrate acid ligands.

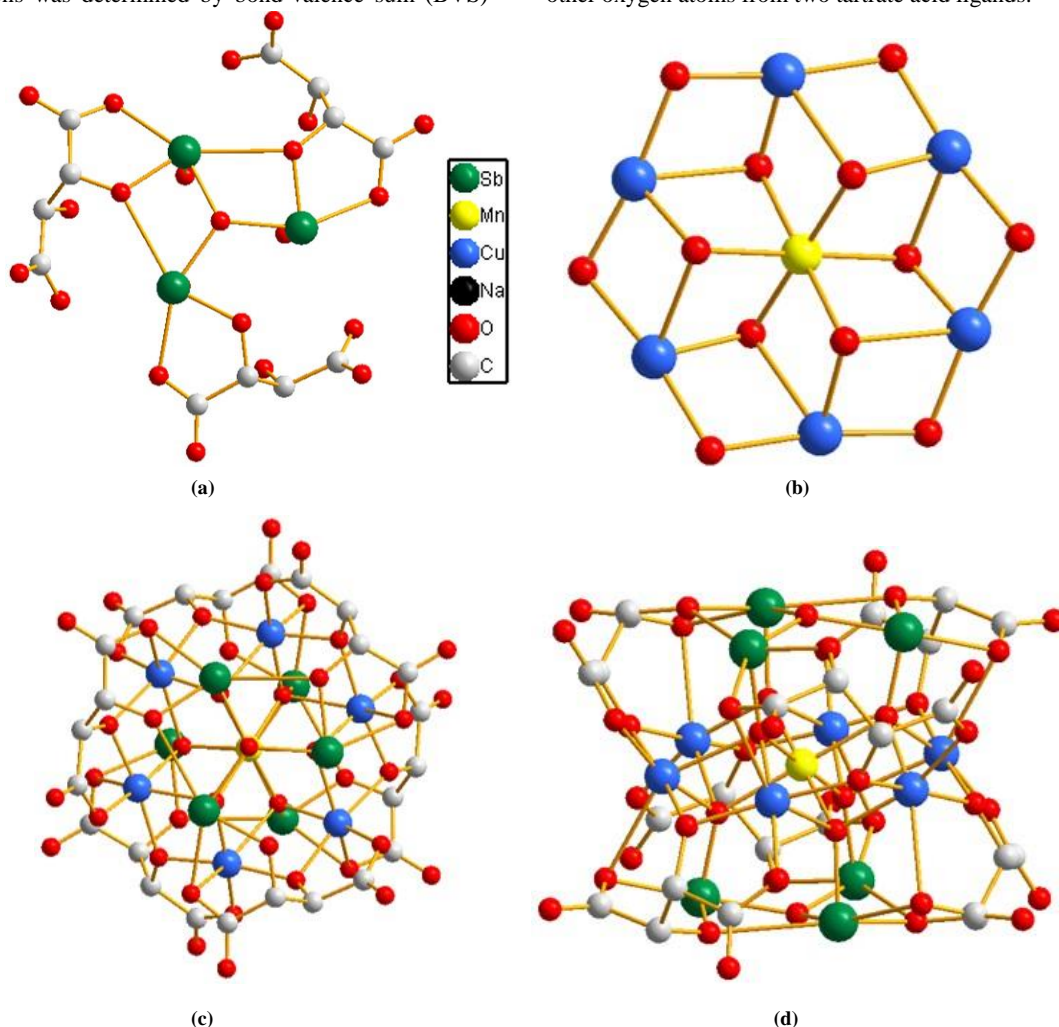


Fig. 1. (a) $\text{Sb}_3(\mu_3\text{-O})(\text{tartrate})_3$ scaffold, (b) $\text{Cu}^{\text{II}}_6\text{Mn}^{\text{III}}$ middle layer, (c) Top view and (d) side view of a ball-and-stick representation of the $\{\text{Cu}_6\text{Mn}\}$ cluster in 1. Color scheme: Cu, blue; Mn, yellow; Sb, green; Na, black; O, red; and C, gray. H atoms are omitted for clarity

Table 2. Bond-valence Sums for the Mn and Cu Atoms of Complexes 1^a

Atom	Mn ^{II}	Mn ^{III}	Atom	Cu ^I	Cu ^{II}
Mn1	2.76	3.01	Cu1	1.70	1.89
			Cu2	1.68	1.87
			Cu3	1.61	1.79

^aThe underlined value is the closest to the charge for which it was calculated.

The oxidation state is the nearest whole number to the underlined value

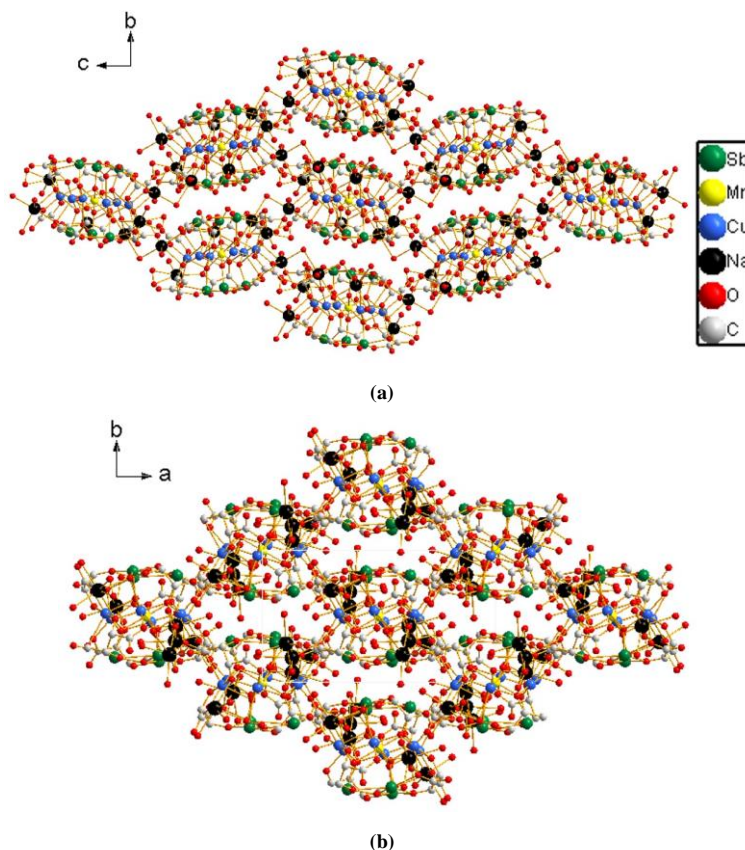


Fig. 2. Ball-and-stick representation of **1**. (a) Packing arrangement viewed along the *a*-axis, (b) Packing arrangement viewed along the *c*-axis. Color scheme: Cu, blue; Mn, yellow; Sb, green; Na, black; O, red; and C, gray. H atoms are omitted for clarity

The Cu^{II}₆Mn^{III} layer is capped by the upper and lower {Sb₃(μ₃-O)} units. In these units, the μ₃-O atom lies in the center of a triangle formed by three Sb^{III} ions. All Sb^{III} cations display the typical one-sided coordination environment expected for lone-pair cations^[26]. Four Sb^{III} cations are coordinated with five oxygen atoms in a distorted tetragonal pyramidal arrangement with four strong Sb–O bonds (1.966~2.387 Å) and one weak Sb–O bond (2.807~2.808 Å), while another two Sb^{III} cations coordinate to four oxygen atoms with four strong Sb–O bonds (1.945~2.307 Å). As a 4-connected node, each cluster is interlinked to its nearest

four {Cu₆Mn} neighbors through the Na(1) and Na(3) cations, generating a three-dimensional supramolecular framework (Fig. 2).

3.2 Infrared spectra of **1**

Infrared spectrum of complex **1** demonstrates a very intense band at about 3400 cm⁻¹ ascribed to the characteristic absorption peaks of O–H stretching vibrations^[27]. In addition, the peaks at 1613 and 1366 cm⁻¹ are attributed to asymmetrical and symmetrical stretching vibrations of -COOH from tartaric acid ligands, respectively^[28].

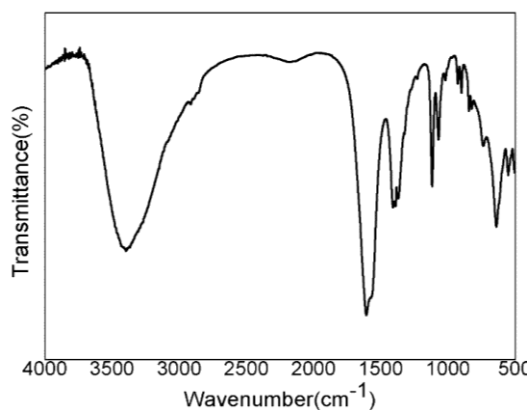


Fig. 3. Fourier transforms infrared spectrum of compound **1**

3.3 Powder X-ray diffraction (PXRD) and thermogravimetric analysis of **1**

In order to check phase purity of complex **1**, the sample was characterized by PXRD at room temperature. As reported in Fig. 4a, the peak positions of the simulated and experimental PXRD patterns are consistent with each other, which were confirmed high phase purity of the as-synthesized samples. The slight difference in intensity for experimental and simulated powder diffraction data may be caused by the preferred orientation of the crystalline powder

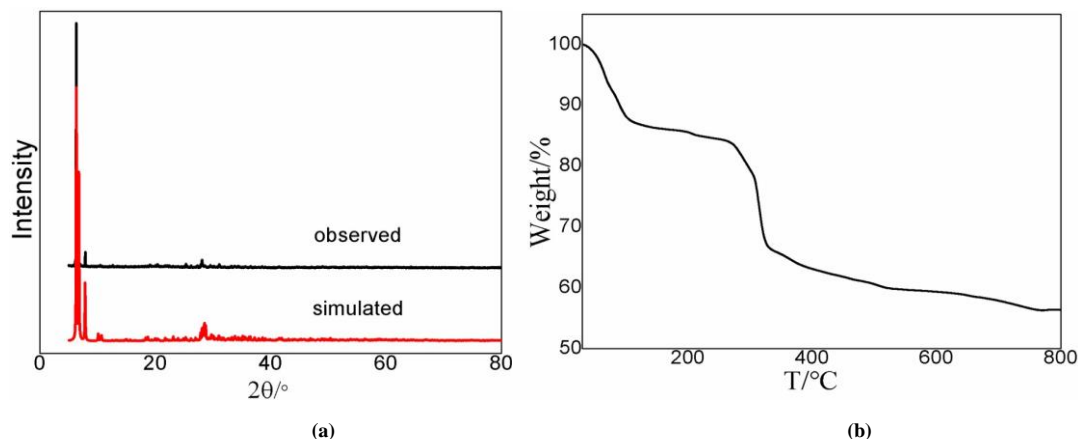


Fig. 4. (a) Comparison of stimulated (red) and experimental (black) powder XRD patterns of complex **1**, (b) Thermogravimetric curves for complex **1**

3.4 Magnetic property

Magnetic susceptibility of **1** was measured in a temperature range of 5~300 K with field of 1 kOe. Plot of the temperature dependence of $\chi_M T$ vs T for **1** is shown in Fig. 5. The room temperature $\chi_M T$ value of **1** is $5.55 \text{ cm}^3 \cdot \text{K} \cdot \text{mol}^{-1}$, which is almost the same as the expected spin-only ($g = 2.0$) value of $5.50 \text{ cm}^3 \cdot \text{K} \cdot \text{mol}^{-1}$ for one Mn^{III} ($S = 2$) and six respective Cu^{II} ions ($S = 1/2$). Upon lowering the temperature, the $\chi_M T$ value decreases rapidly from room

samples.

The thermogravimetric analysis of complex **1** under N_2 atmosphere from 30 to 800 °C at a heating rate of 10 °C/min is shown in Fig. 4b. The initial weight loss process occurs from room temperature to 260 °C, which can be assigned to the release of the free and lattice water molecules (obsd.: 15.36%, calcd.: 13.41%). As the temperature is increased beyond 260 °C, a sharp increase in the weight loss occurs, indicating the decomposition of the tartrate acid ligands.

temperature to $1.76 \text{ cm}^3 \cdot \text{K} \cdot \text{mol}^{-1}$ at 25 K and then drops gradually to $1.56 \text{ cm}^3 \cdot \text{K} \cdot \text{mol}^{-1}$ at 5.0 K, indicating dominating antiferromagnetic interactions. The above data were fitted to the spin Hamiltonian in Eq. 1 using the program PHI^[29], which gives $g_{\text{Cu}} = 2.26$, $g_{\text{Mn}} = 1.98$, $J_{\text{Cu-Cu}} = 176.34 \text{ cm}^{-1}$ and $J_{\text{Cu-Mn}} = -14.44 \text{ cm}^{-1}$ ($S_1 = S_2 = S_3 = S_4 = S_5 = S_6 = S_{\text{Cu}}$, $S_7 = S_{\text{Mn}}$). Two exchange pathways of Cu-Cu and Cu-Mn can be seen clearly in the asymmetric unit.

$$H = -2J_1(S_1S_2 + S_2S_3 + S_3S_4 + S_4S_5 + S_5S_6) - 2J_2(S_1S_7 + S_2S_7 + S_3S_7 + S_4S_7 + S_5S_7 + S_6S_7) \quad (1)$$

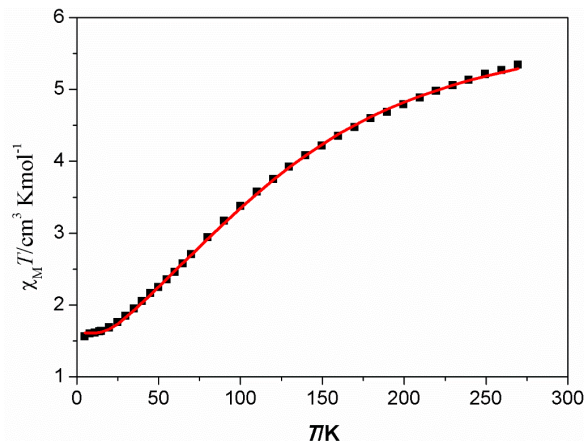


Fig. 5. $\chi_M T$ (•) vs T plots for **1**. The red line represents the best fit using the spin-Hamiltonian

4 CONCLUSION

In conclusion, we have presented a new transition metal-antimony oxo-cluster constructed by a Cu^{II}₆Mn^{III} middle layer capping by two {Sb₃(μ₃-O)} scaffolds and six tartrate acid ligands from the aqueous medium under mild

conditions. In addition, the magnetic property of **1** was investigated, indicating dominating antiferromagnetic couplings with $J_{\text{Cu-Cu}} = 176.34$ and $J_{\text{Cu-Mn}} = -14.44 \text{ cm}^{-1}$. The work to design and synthesize new transition metal-antimony oxo-cluster is in progress.

REFERENCES

- (1) Zhang, Y. Y.; Gao, W. X.; Lin, L.; Jin, G. X. Recent advances in the construction and applications of heterometallic macrocycles and cages. *Coord. Chem. Rev.* **2017**, 344, 323–344.
- (2) Ma, W.; Hu, B.; Jing, K. Q.; Li, Z.; Jin, J. C.; Zheng, S. T.; Huang, X. Y. Proton-conducting layered structures based on transition metal oxo-clusters supported by Sb(III) tartrate scaffolds. *Dalton Trans.* **2020**, 49, 3849–3855.
- (3) Sun, Y. Y.; Lu, D. F.; Sun, Y. X.; Gao, M. Y.; Zheng, N.; Gu, C.; Wang, F.; Zhang, J. Large titanium-oxo clusters as precursors to synthesize the single crystals of Ti-MOFs. *ACS Materials Lett.* **2021**, 3, 64–68.
- (4) Chen, W. T. A one-dimensional manganese(III)-porphyrin coordination polymer: crystal structure and photophysical properties. *Acta Crystallogr. C* **2020**, 76, 375–380.
- (5) Tan, Y. X.; Wang, F.; Zhang, J. Design and synthesis of multifunctional metal-organic zeolites. *Chem. Soc. Rev.* **2018**, 47, 2130–2144.
- (6) Chen, W. T. Structure, photophysical and electrochemical properties of a copper porphyrin with a three-dimensional framework. *Acta Crystallogr. C* **2020**, 76, 133–138.
- (7) Tan, H. H.; Lv, X. L.; Liu, J. L.; Cheng, Y. F.; Zhou, Q. L.; Lin, Y. T.; Meng, W. A 2D layer copper(II) coordination polymer with 3-nitrophthalic acid: synthesis, crystal structure and copper 3-nitrophthalate metal-organic framework-graphene oxide nanocomposite. *Chin. J. Struct. Chem.* **2021**, 40, 459–464.
- (8) O'Connor, H. M.; Sanz, S.; Scott, A. J.; Pitak, M. B.; Klooster, W. T.; Coles, S. J.; Chilton, N. F.; McInnes, E. J. L.; Lusby, P. J.; Weihe, H.; Piligkos, S.; Brechin, E. K. [Cr^{III}₈Ni^{II}₆]⁹⁺ heterometallic coordination cubes. *Molecules* **2021**, 26, 757–766.
- (9) Dutta, S.; Ghosh, T. K.; Mahapatra, P.; Ghosh, A. Joining of trinuclear heterometallic Cu^{II}–M^{II} (M = Mn, Cd) nodes by nicotinate to form 1D chains: magnetic properties and catalytic activities. *Inorg. Chem.* **2020**, 59, 14989–15003.
- (10) Diego, R.; Pavlov, A.; Darawsheh, M.; Aleshin, D.; Nehrkorn, J.; Nelyubina, Y.; Roubeau, O.; Novikov, V.; Aromí, G. Coordination [Co^{II}₂] and [Co^{II}Zn^{II}] helicates showing slow magnetic relaxation. *Inorg. Chem.* **2019**, 58, 9562–9566.
- (11) Kobayashi, F.; Ohtani, R.; Kusumoto, S.; Lindoy, L. F.; Hayami, S.; Nakamura, M. Wheel-type heterometallic ferromagnetic clusters: [Ni₇-XM_x(HL)₆(μ₃-OMe)₄(μ₃-OH)₂]Cl₂ (M = Zn, Co, Mn; x = 1, 3). *Dalton Trans.* **2018**, 47, 16422–16428.
- (12) Stetsiuk, O.; Synytsia, V.; Petrusenko, S. R.; Kokozay, V. N.; El-Ghayoury, A.; Cano, J.; Lloret, F.; Julve, M.; Fleury, B.; Avarvari, N. Co-existence of ferro- and antiferromagnetic interactions in a hexanuclear mixed-valence Co^{III}₂Mn^{II}₂Mn^{IV}₂ cluster sustained by a multidentate Schiff base ligand. *Dalton Trans.* **2019**, 48, 11862–11871.
- (13) Liu, J.; Qu, M.; Cléac, R.; Zhang, X. M. A two-dimensional honeycomb coordination network based on fused triacontanuclear heterometallic {Co¹²Mn¹⁸} wheels. *Chem. Commun.* **2015**, 51, 7356–7359.
- (14) Milway, V. A.; Tuna, F.; Farrell, A. R.; Sharp, L. E.; Parsons, S.; Murrie, M. Directed synthesis of {Mn₁₈Cu₆} heterometallic complexes. *Angew. Chem. Int. Ed.* **2013**, 52, 1949–1952.
- (15) Dutta, S.; Bhunia, P.; Mayans, J.; Drew, M. G. B.; Ghosh, A. Roles of basicity and steric crowding of anionic coligands in catechol oxidase-like activity of Cu(II)–Mn(II) complexes. *Dalton Trans.* **2020**, 49, 5730–5735.
- (16) Grancha, T.; Mon, M.; Lloret, F.; Ferrando-Soria, J.; Jourmaux, Y.; Pasán, J.; Pardo, E. Double interpenetration in a chiral three-dimensional magnet with a (10,3)-a structure. *Inorg. Chem.* **2015**, 54, 8890–8892.
- (17) Liu, K.; Shi, W.; Cheng, P. Toward heterometallic single-molecule magnets: synthetic strategy, structures and properties of 3d-4f discrete complexes. *Coord. Chem. Rev.* **2015**, 74–122.
- (18) Meng, W.; Deng, Y. M.; Xu, F. Facile and environmentally friendly one-step synthesis of hexanuclear Cu(II)–Ni(II) and Cu(II)–Co(II) clusters and their binding interactions with bovine serum albumin. *J. Solid State Chem.* **2021**, 295, 121904–121912.
- (19) Meng, W.; Xu, F.; Xu, W. J. An anionic heptacopper(II) oxo-cluster {Cu^{II}₇} with an $S = 7/2$ ground state. *Inorg. Chem.* **2016**, 55, 540–542.

- (20) Gao, Q.; Wang, X. Q.; Tapp, J.; Moeller, A.; Jacobson, A. J. Antimony tartrate transition-metal-oxo chiral clusters. *Inorg. Chem.* **2013**, 52, 6610–6616.
- (21) Gao, Q.; Wang, X. Q.; Jacobson, A. J. A homochiral diamond framework constructed from Fe(III) and Mn(II) oxo-clusters supported by Sb(III) tartrate scaffolds. *Chem. Commun.* **2012**, 48, 3990–3992.
- (22) Gao, Q.; Wang, X. Q.; Conato, M. T.; Makarenko, T.; Jacobson, A. J. Microporous, homochiral structures containing iron oxo-clusters supported by antimony(III) tartrate scaffolds. *Cryst. Growth Des.* **2011**, 11, 4632–4638.
- (23) Sheldrick, G. M. *SHELXS-97, Program for X-ray Crystal Structure Solution*. University of Göttingen, Germany **1997**.
- (24) Henkelis, J. J.; Jones, L. F.; Miranda, M. P.; Kilner, C. A.; Halcrow, M. A. Two heptacopper(II) disk complexes with a $[\text{Cu}_7(\mu_3\text{-OH})_4(\mu\text{-OR})_2]^{8+}$ core. *Inorg. Chem.* **2010**, 49, 11127–11132.
- (25) Evans, H. T. Jr. The crystal structures of ammonium and potassium molybdotellurates. *J. Am. Chem. Soc.* **1948**, 70, 1291–1292.
- (26) Ugandhar, U.; Navaneetha, T.; Ali, J.; Mondal, S.; Vaitheeswaran, G.; Baskar, V. Assembling homometallic Sb_6 and heterometallic Ti_4Sb_2 oxo clusters. *Inorg. Chem.* **2020**, 59, 6689–6696.
- (27) Fan, L. M.; Gao, L. L.; Wang, X. Q.; Wang, J.; Zhao, L.; Fang, K. G.; Hua, T. P. Structural diversity and magnetic properties of four Cu(II)/Co(II) coordination complexes based on 3,5-bis(2-carboxylphenoxy)benzoic acid. *Polyhedron* **2018**, 141, 133–139.
- (28) Li, C. H.; Kuang, Y. F.; Li, W.; Li, Y. L. Hydrothermal synthesis, crystal structure and properties of a new binuclear cage-like yttrium(III) complex $\text{Y}_2(\text{TMBA})_6(\text{phen})_2$. *Chin. J. Struct. Chem.* **2020**, 39, 2016–2020.
- (29) Chilton, N. F.; Anderson, R. P.; Turner, L. D.; Soncini, A.; Murray, K. S. PHI: a powerful new program for the analysis of anisotropic monomeric and exchange-coupled polynuclear *d*- and *f*-block complexes. *J. Comput. Chem.* **2013**, 34, 1164–1175.